NeuroImage 177 (2018) 88–97

Contents lists available at ScienceDirect

NeuroImage

journal homepage: www.elsevier.com/locate/neuroimage

Contributions of dopaminergic and non-dopaminergic neurons to VTA-stimulation induced neurovascular responses in brain reward circuits

Marta Brocka [a], Cornelia Helbing [b], Daniel Vincenz [a], Thomas Scherf [a], Dirk Montag [c], Jürgen Goldschmidt [a], Frank Angenstein [b,d,e,1], Michael Lippert [a,*,1]

[a] Department Systems Physiology of Learning, Leibniz Institute for Neurobiology, Magdeburg, Germany
[b] Functional Neuroimaging Group, Deutsches Zentrum für Neurodegenerative Erkrankungen (DZNE), Magdeburg, Germany
[c] Neurogenetics, Leibniz Institute for Neurobiology, Magdeburg, Germany
[d] Center for Behavioral Brain Science (CBBS), Magdeburg, Germany
[e] Medical Faculty, Otto-von-Guericke University, Magdeburg, Germany

ARTICLE INFO

Keywords:
Optogenetics
BOLD
Dopamine
Ventral tegmental area
Nucleus accumbens
rCBF

ABSTRACT

Mapping the activity of the human mesolimbic dopamine system by BOLD-fMRI is a tempting approach to non-invasively study the action of the brain reward system during different experimental conditions. However, the contribution of dopamine release to the BOLD signal is disputed. To assign the actual contribution of dopaminergic and non-dopaminergic VTA neurons to the formation of BOLD responses in target regions of the mesolimbic system, we used two optogenetic approaches in rats. We either activated VTA dopaminergic neurons selectively, or dopaminergic and mainly glutamatergic projecting neurons together. We further used electrical stimulation to non-selectively activate neurons in the VTA. All three stimulation conditions effectively activated the mesolimbic dopaminergic system and triggered dopamine releases into the NAcc as measured by *in vivo* fast-scan cyclic voltammetry. Furthermore, both optogenetic stimulation paradigms led to indistinguishable self-stimulation behavior. In contrast to these similarities, however, the BOLD response pattern differed greatly between groups. In general, BOLD responses were weaker and sparser with increasing stimulation specificity for dopaminergic neurons. In addition, repetitive stimulation of the VTA caused a progressive decoupling of dopamine release and BOLD signal strength, and dopamine receptor antagonists were unable to block the BOLD signal elicited by VTA stimulation. To exclude that the sedation during fMRI is the cause of minimal mesolimbic BOLD in response to specific dopaminergic stimulation, we repeated our experiments using CBF SPECT in awake animals. Again, we found activations only for less-specific stimulation. Based on these results we conclude that canonical BOLD responses in the reward system represent mainly the activity of non-dopaminergic neurons. Thus, the minor effects of projecting dopaminergic neurons are concealed by non-dopaminergic activity, a finding which highlights the importance of a careful interpretation of reward-related human fMRI data.

Introduction

The ventral tegmental area (VTA) is a major source of dopamine in the brain and as central part of the mesolimbic dopamine system involved in learning, reward processing, addiction and motivation (Ungless et al., 2010; Volman et al., 2013; Wise and Koob, 2014). Even though the anatomical connections of the VTA have been broadly studied (Beier et al., 2015; Hnasko et al., 2012; Li et al., 2009; Sanchez-Catalan et al., 2014; Taylor et al., 2014; Walsh and Han, 2014; Yetnikoff et al., 2014), and the association of dopaminergic projections from VTA to nucleus accumbens with reward prediction error has been established (Beier et al., 2015; Schultz et al., 1997; Steinberg et al., 2013), the effects of VTA dopamine release on neurovascular responses at the whole brain level remain highly controversial (Decot et al., 2016; Ferenczi et al., 2016; Helbing et al., 2016; Lohani et al., 2016). In case of the VTA it is particularly difficult to infer resulting neurovascular effects from anatomical connections, as dopamine is a neuromodulator with a multitude of functionally different receptors (Sokoloff et al., 1988). In addition, the connections of the VTA are widespread, targeting areas which are mutually interconnected, and often not exclusive for one

* Corresponding author. Department of Systems Physiology, Leibniz Institute for Neurobiology, Brenneckestrasse 6, Magdeburg, Germany.
E-mail address: mlippert@lin-magdeburg.de (M. Lippert).
[1] These authors contributed equally.

https://doi.org/10.1016/j.neuroimage.2018.04.059
Received 4 January 2018; Received in revised form 11 April 2018; Accepted 25 April 2018
Available online 30 April 2018

neurotransmitter (Beier et al., 2015). Nonetheless, since the VTA with its dopaminergic projections to nucleus accumbens (NAcc) plays such a central role for behavior, their activity and functional connectivity have been subject to numerous human fMRI studies. BOLD responses in these areas are often interpreted as a signal of reward related dopamine release (Honey et al., 2003; Knutson and Gibbs, 2007; Kufahl et al., 2005; Schott et al., 2008; Vytlacil et al., 2014). If nucleus accumbens BOLD responses indeed faithfully report this activity, fMRI would provide an invaluable tool to non-invasively study human reward processing.

As a relatively new method, optogenetics allows selective activation of dopaminergic VTA neurons, which in principle permits directly testing this link between VTA dopamine release and BOLD. Unsurprisingly, several studies have addressed the issue recently (Ferenczi et al., 2016; Helbing et al., 2016; Lohani et al., 2016). First, results showed significant BOLD signal changes in response to optogenetic VTA stimulation but the magnitude of the BOLD response was low. Here, we thus ask the question of how these signals correspond to reward-related, canonical BOLD signals observed in humans.

We tested three stimulation paradigms, differing in their specificity for dopaminergic neurons in the VTA: electrical VTA stimulation, 'less-specific' optogenetic VTA stimulation targeting CamKIIa-positive VTA neurons, comprising both glutamatergic and dopaminergic cells (Guo et al., 2014) and 'specific' optogenetic stimulation of dopaminergic neurons in Th-Cre rats. Using a dopamine receptor antagonist we further tested a possible contribution of dopamine to stimulus induced BOLD signal changes seen during less-specific stimulation. We also quantified the release of dopamine using fast scan cyclic voltammetry (FSCV) in the different paradigms and tested the animals in an optogenetic intracranial self-stimulation paradigm (optoICSS) to confirm the behavioral equivalence of the two optogenetic stimulation paradigms and underlying dopamine release.

In contrast to human fMRI studies, animal fMRI studies are often performed under sedation or anesthesia (Lohani et al., 2016). We therefore complemented our fMRI measurements, which were performed under sedation, with a novel technique for SPECT imaging of regional cerebral blood flow in awake, freely moving animals (rCBF SPECT; Kolodziej et al., 2014; Vincenz et al., 2017) to exclude sedation-related effects.

Materials and methods

Subjects

Rats were housed under standard laboratory conditions (constant temperature, 12:12 h light/dark cycle, food and tap water ad libidum). Both transgenic Th-Cre rats and their non-transgenic littermates (Long Evans-Tg (Th::Cre)3.1Deis; Witten et al., 2011) were used in the optogenetic experiments. Electrical stimulation data was acquired in Wistar rats. The experiments were performed according to EU Directive 2010/63/EU for animal experiments and approved by the local ethical committee.

Viral vectors and stereotactic surgery

In this study, the following types of viral vectors were used: AAV2/5-CamKIIα-C1V1(E162T)-p2A-EYFP (Prakash et al., 2012) for wild type (WT) animals, AAV2/5-Ef1a-DIO-hChR2(H134R)-EYFP-WPRE-pA for Th-Cre rats and AAV2/5-CaMKIIα-EYFP for WT controls. The CamKIIa-promoter targets a mixed population of VTA neurons, which are predominantly dopaminergic, but not exclusively so (Guo et al., 2014; Helbing et al., 2016). In transgenic animals, selectivity is provided by the expression of Cre-recombinase under the Th-promoter, which is exceptionally specific in the used rat strain (Witten et al., 2011). The two different opsins were used due to their ability to match self-stimulation rates across groups and for consistency with previous work (Helbing et al., 2016). Viral solutions were kindly provided by Karl Deisseroth through the Viral Vector Core of the University of North Carolina.

For virus injection and optical fiber implantation animals were anesthetized with pentobarbital (50 mg/kg) and fixed in a robotic stereotaxic instrument (Neurostar). Two injections of 650 nl viral solution ($2 \times 10E12$ gc/ml) each were conducted unilaterally in the left VTA (−5.8 mm AP, −0.7 mm ML, 7.2 mm for the first injection and 7.6 mm for the second injection DV, speed 100 nl/min, 5–10 min rest after injection). We chose unilateral stimulation to allow detecting contralateral effects of stimulation, which might be opposed in sign to ipsilateral effects. A custom-made optical fiber (200 μm core diameter, N.A. 0.39) was implanted above the injection sites (6.8 mm DV). Rats were given at least three weeks to recover and to express the virus.

Implantation of the electrodes

Electrical VTA stimulation was performed as previously described (Helbing et al., 2016). Briefly, rats were deeply anesthetized with pentobarbital (40 mg/kg, i.p.) and placed in a stereotactic frame. For electrical stimulation, a bipolar stimulation electrode was implanted in the VTA (coordinates: AP -5.6 mm, ML +2.3 mm from Bregma, DV 7.8 mm from dural surface angled 10° to the midline). During implantation, brief stimulation bursts (10 pulses, ISI 10 ms, 300 μA) were delivered and the electrode placed in a location, where it evoked clear whisker movements (Kunori et al., 2014; Solt et al., 2014; Taylor et al., 2016). Following surgery, animals were provided with *ad libitum* food and water and housed individually for a recovery period of 1 week.

ICSS

To confirm correct fiber placement, animals were trained in an intracranial self-stimulation (ICSS) paradigm for 10 consecutive days (30 min/day). Upon pressing the nosepoke lever, the rat received a brief train of laser light pulses (10 pulses, 25 Hz, 10 ms pulse width, 10 mW at the tip of the fiber, WT: 532 nm, Th-Cre: 473 nm). Animals that did not reach 400 presses per session after 10 days were not used further in the study. This approach avoids false negative results, since substantial dopamine release was present in each scanned animal.

fMRI

MRI in combination with optogenetic or electrical stimulation of the VTA was performed as previously described (Helbing et al., 2016). Rats were initially anesthetized with isoflurane (1.5%; in 50:50 N_2:O_2; v:v) and fixed into the head holder. Depending on the experiment, they were either connected to recording and stimulation electrodes (electrical stimulation) or to the optical cable (optogenetic stimulation). The anesthesia was switched to deep sedation by application of medetomidine (Dorbene, Pfizer GmbH, bolus: 50 μg/kg s.c. and after 15 min 100 μg/kg per h s.c.; (Weber et al., 2006). Breathing, heart rate and oxygen saturation were monitored throughout the experiment by an MRI-compatible pulse oxymeter (MouseOX™; Starr Life Sciences Corp., Pittsburgh, PA, USA). Heating was provided from the ventral site.

All fMRI measurements were performed on a 4.7T Bruker Biospec 47/20 animal scanner (free bore of 20 cm) equipped with BGA09 (400 mT/m) gradient system (Bruker BioSpin GmbH, Ettlingen, Germany). A 50 mm Litzcage small animal imaging system (DotyScientific Inc., Columbus, SC, USA) was used for the RF signal reception.

Anatomical T_2-weighted spin-echo images were obtained using a rapid acquisition relaxation enhanced (RARE) sequence with the following parameters: TR 4000 ms, TE 15 ms, RARE factor 8, 10 horizontal slices, slice thickness 0.8 mm, FOV 37×37 mm, matrix 256×256, number of averages 4. The total scanning time was 8 min 32 s. Functional MRI (fMRI) was performed using a gradient-echo EPI (echo planar imaging) sequence with the following parameters: TR 2000 ms, TE 24 ms, matrix 92×92. The slice geometry, i.e., ten horizontal slices, was identical to the previously obtained anatomical spin-echo-images.

Optogenetic stimulation

Every stimulation protocol was preceded with 2 min baseline acquisition, during which no stimulation was applied. We used the same fMRI optical stimulation protocol as previously described (Helbing et al., 2016). Briefly, it consists of 8 bursts of light (10 pulses, 25 Hz, 10 ms, 10 mW, 532 nm in case less-specific stimulation, 473 nm in case of specific stimulation and EYFP control rats), spaced 1 s apart and followed by 52 s of rest. This sequence was repeated 15 times for each animal. Total scanning time was therefore 17 min. For the fMRI measurements 11 WT, 10 Th-Cre and two control animals were used.

Electrical stimulation

During fMRI the VTA was stimulated with discontinuous 100 Hz pulses, i.e., 8 bursts of 10 pulses applied one burst per second. One stimulation train lasted 8 s, so during the one train 80 identical pulses were applied (Fig. 1 D). The applied stimulation protocol consisted of 10 consecutive stimulation trains, given every minute after the 2-min baseline. The pulse intensity for the VTA stimulation was set to 300 μA, which did not cause clear stimulus-dependent movements of the head.

Pharmacological interference

To test the influence of the dopamine $D_{1/5}$ receptor blockade on the formation of BOLD response during optogenetic stimulation, the dopamine $D_{1/5}$-receptor antagonist SCH23390 was injected intraperitoneally 30 min prior to stimulation and scanning (0.2 mg/kg). This dose was selected to minimize off-target effects of the drug at vascular monoamine receptors (Ohlstein and Berkowitz, 1985) and, when systemically applied, to be still sufficient to affect dopamine-related spontaneous theta burst activity (Fitch et al., 2006) or cocaine-induced changes in rCBV (Marota et al., 2000). The stimulation and scanning followed the standard protocol described above.

Data processing and analysis

The fMRI data was analyzed in BrainVoyager QX2.6.1 (Brain Innovation, Maastricht, the Netherlands). A standard sequence of preprocessing steps, including slice scan time correction, 3D motion

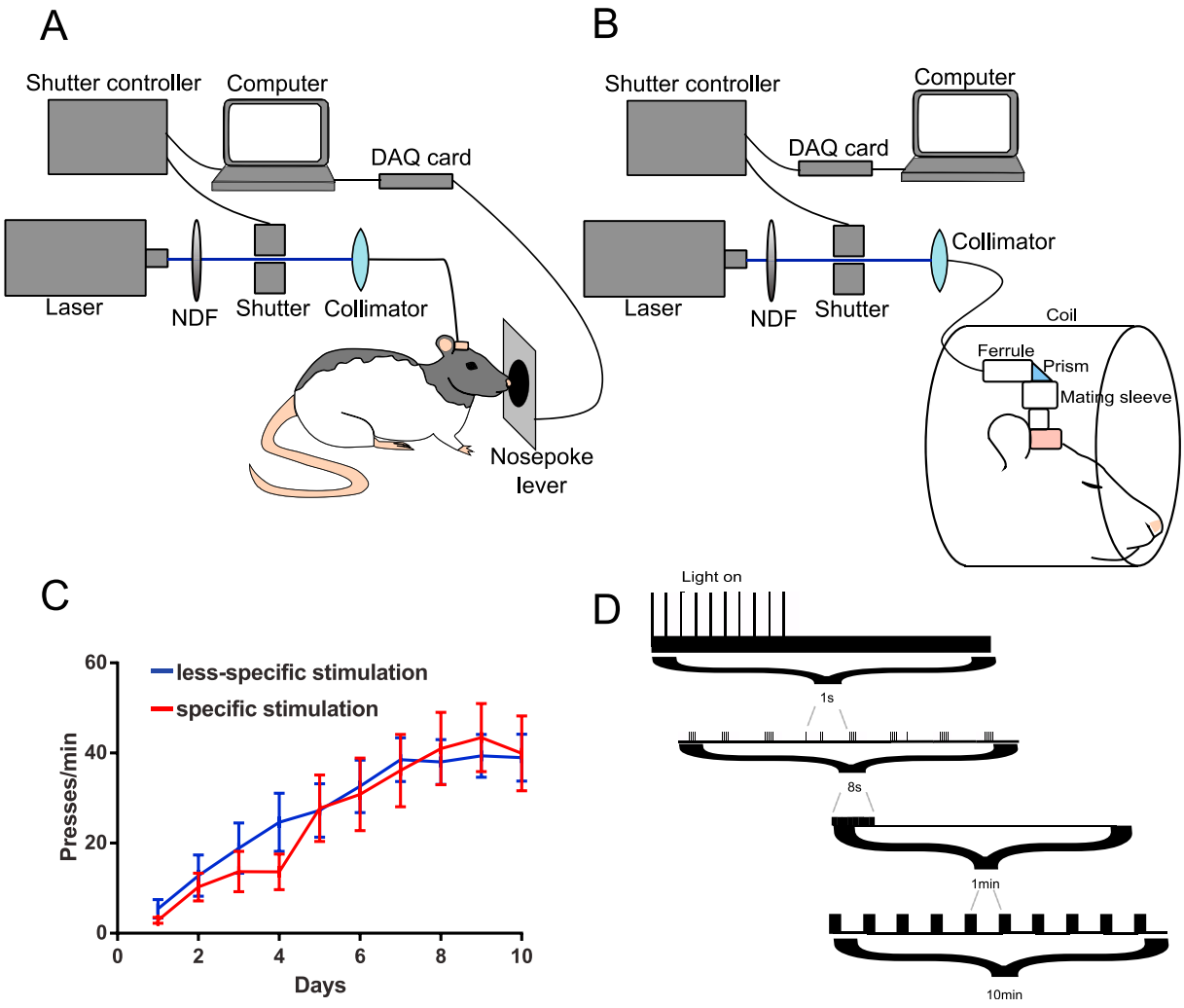

Fig. 1. A: Self-stimulation setup. The animal has access to a self-stimulation nose poke lever. Upon pressing this lever, a computer delivers a train of laser light pulses. The DPSS laser is kept in CW mode and optically shuttered to ensure precise optical pulse power. B: Setup for optogenetic stimulation during fMRI. The animal is sedated and placed in the fMRI scanner. Light delivery is achieved through the same optical setup used for self-stimulation. A custom-made light coupler is used to guide the light into the narrow volume coil without excessive fiber bending. A microscopic prism is used to deflect the light 90° into the fiber implant of the animal. C: ICSS training results. Animals acquired self-stimulation similarly for specific optogenetic stimulation as well as less-specific stimulation. D: fMRI and SPECT optogenetic pulse sequence. Stimulation consists of 8 bursts of light each containing 10 pulses delivered at 25 Hz, spaced 1 s apart and followed by 52 s of no stimulation. The sequence is repeated once per minute for 15 times (fMRI) or 10 times (SPECT).

correction (trilinear interpolation and reduced data using the first volume as reference) and temporal filtering (high pass GLM-Fourier: three sines/cosines and Gaussian filter; FWHM 3 data points) was applied to each data set. Images were reconstructed at 128 × 128 voxels per slice and spatially smoothed (Gaussian filter of 1.4 voxel). Functional activation was analyzed by using the correlation of the observed BOLD signal intensity changes in each voxel with a predictor (hemodynamic response function- HRF), generated from the given stimulus protocol (see above). To calculate the predictor, the square wave representing stimulus on and off conditions was convolved with a double gamma HRF (onset 0s, time to response peak 5s, time to undershoot peak 15s). Based on this multi subject GLM (general linear model) analysis the appropriate activation map could be generated. All significantly activated voxels were converted into volumes of interest (VOI), from which surface clusters were created and visualized with the BrainVoyager VOI analysis tool. To exclude false positive voxels, we only considered those with a significance level p above the threshold set by Bonferroni corrected p value of 0.001 (which corresponds to a t value greater than 5.6) or by an uncorrected p value of 0.01 (which corresponds to a t value greater than 3.2). Averaged BOLD time series of individual clusters of activation are summarized in Fig. 2.

In addition a volume of interest (VOI) analysis was performed. Individual VOIs, i.e., right and left hippocampus, right and left nucleus accumbens, right and left striatum, septum, prefrontal cortex region and VTA were marked in the 3D standard rat brain. The average BOLD time series of all voxels located in one VOI was then calculated for each individual animal using the volume-of-interest-analysis tool implemented in the BrainVoyager QX2.6.1 software. Each individual BOLD time series was normalized using the averaged BOLD signal intensity as 100%. All normalized BOLD time series were then averaged and depicted as mean BOLD time series ± SD. These mean BOLD time series of individual VOIs were used to calculate event related BOLD responses.

Event-related BOLD responses were calculated by measuring the signal intensities starting six frames before stimulus onset (−12 s until 0 s), during stimulus presentation (between 0 and 8s, which corresponds to four frames) and the following 15 frames (8s–38s) after the end of the stimulus. To avoid the confounding effect of putative variations in baseline BOLD signal intensities on the calculated BOLD response (i.e. $\text{BOLD signal}_{\text{stimulus}}/\text{BOLD signal}_{\text{baseline}} \times 100\%$), each BOLD response was related to BOLD signal intensities of the stimulus over the preceding 12s.

Second-level group analysis

To visualize significant differences in BOLD responses between the control and SCH23390 treated rats, a fixed effect analysis with a general linear model (GLM)—including z-transformed functional data of all animals—was performed using the 2-gamma response function implemented in BrainVoyager™QX. Correction for serial correlation was performed using a second order autoregressive model (Goebel, 2012). To

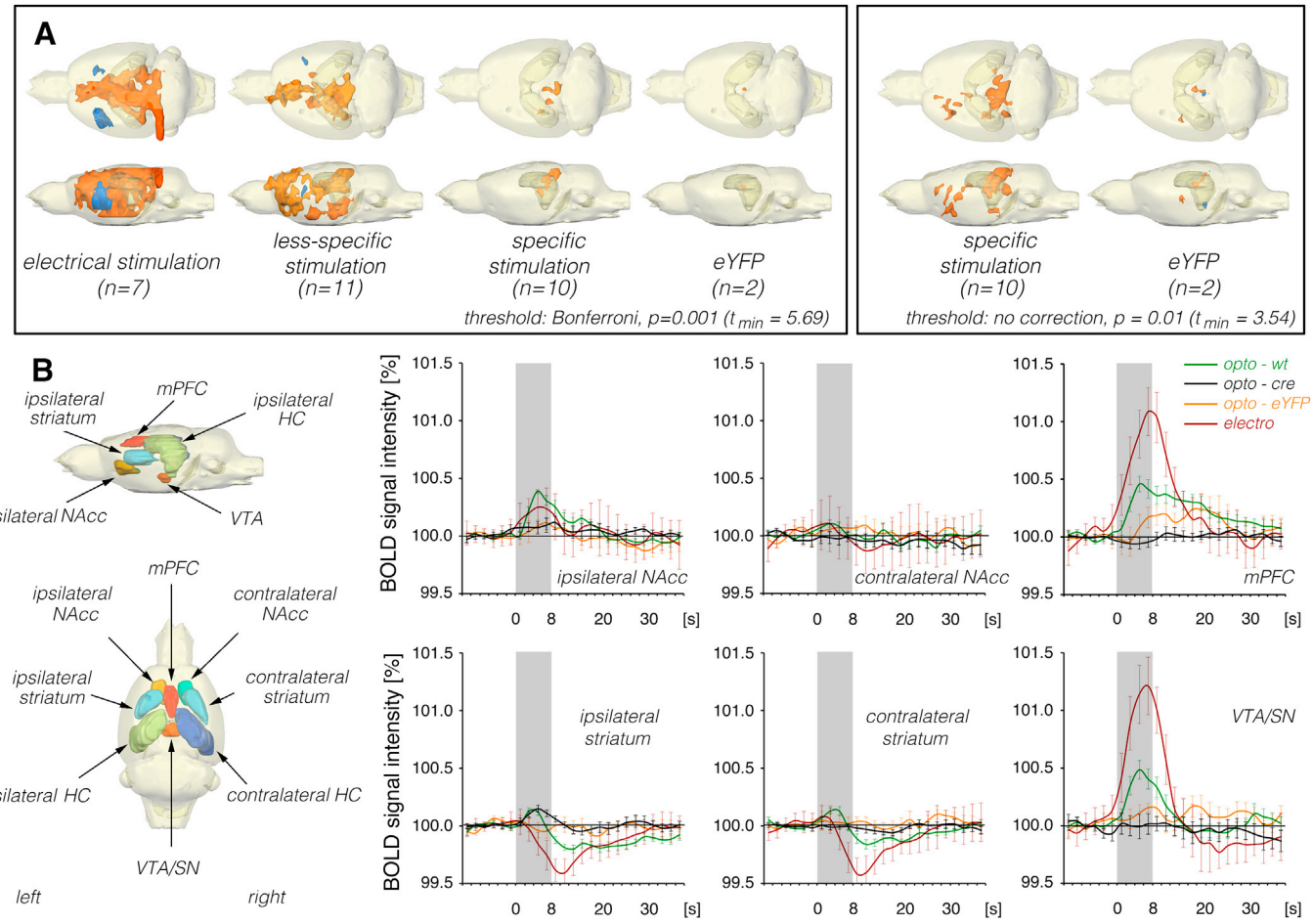

Fig. 2. BOLD response pattern during electrical and optogenetic stimulation of the VTA. A: Spatial distribution of significantly activated voxels. Electrical stimulation and less-specific optogenetic stimulation of the VTA caused widespread BOLD responses in various brain regions. Specific optogenetic stimulation of VTA dopaminergic cells only led to minor BOLD responses, mainly in the tectal area. Responses in reward related areas were only detectable if the statistical threshold was lowered and no correction for multiple testing performed (right panel). B: Magnitude of BOLD responses in individual brain structures (i.e., volumes of interest VOI). BOLD time series in selected VOIs are shown averaged across all voxels and repetitions (gray bar: stimulation duration).

visualize regions that were affected in their activities after application of a dopaminergic antagonist, differences in BOLD signal intensities between the two conditions (i.e., control > SCH23390 treated) were computed ($t \geq 5.2$; Bonferroni P value: 0.01; cluster threshold 0.15 mm^3). All significantly activated voxels were converted into volumes of interest (VOI), from which surface clusters were created and visualized with the BrainVoyager VOI analysis tool.

SPECT-imaging of regional cerebral blood flow

Following fMRI scans, animals were implanted with a silicon catheter in the right external jugular vein (Gaudig Laborfachhandel GbR, Sülzetal-Osterwedding, Germany; OD: 1.3 mm, ID: 0.5 mm, catheter length 11 cm). Catheter lock solution (Cath-Loc HGS, SAI Infusion Technologies, USA) was injected into the catheter to prevent clogging. The animals were given at least one day to recover from surgery before the SPECT measurements. 9 WT and 9 Cre rats, which previously underwent the fMRI experiment, were used (3 animals were excluded due to catheter block). For each animal, a baseline and stimulation measurement was performed.

Animals were awake during the injection of the radioactive tracer (250 MBq of ^{99m}Tc-HMPAO in 400 µl volume, for details see Kolodziej et al., 2014 and Vincenz et al., 2017).

In both stimulation conditions, animals were connected to the optical cable and could move freely in a plastic box resembling the self-stimulation chamber.

The optical stimulation protocol was similar to the protocol used during fMRI but contained 10 instead of 15 repetitions following previous protocols (Kolodziej et al., 2014) with tracer-injection times of 10 min. After these 10 min, rats were anesthetized with isoflurane and scanned in a small animal SPECT scanner (NanoSPECT/CT, Mediso, Hungary). Images were reconstructed at an isotropic voxel size of 333 µm. In addition to SPECT, CT scans (45 kVp, 177 µA, 180 projections, 500 ms per projection) were acquired from the same FoV as SPECT-images and reconstructed at an isotropic voxel size of 200 µm. SPECT/CT images were aligned to a rat brain MR-template using the MPI-Tool-Software (Advanced Tomo Vision, Germany). Alignments were based on the best fit of CT- and MR-images and all images were saved with 200 µm isotropic voxel sizes. SPECT-brain data were manually segmented using a whole-brain VOI with the Osirix™ software (Pixmeo, Switzerland), version 5.7.

SPECT data sets were intensity-normalized to the same global mean. For statistical analysis, voxelwise paired t-tests were performed. The resulting *P*-maps were smoothed with a median filter using a $3 \times 3 \times 3$ voxel kernel. Statistical analysis and smoothing were done with the Magnan-Software (version 2.4, BioCom GbR, Germany). In accordance with previous small-animal radionuclide imaging studies, uncorrected *P*-values are given (Endepols et al., 2010; Michaelides et al., 2013; Thanos et al., 2013). SPECT/MR fusion images were made in Osirix and arranged for illustration using Photoshop CS6.

Fast-scan cyclic voltammetry (FSCV)

Rats were anesthetized with urethane (1.6 g/kg i.p.) and placed in the stereotactic frame. We used 3 animals for less-specific stimulation and 4 for specific stimulation. A carbon fiber working electrode was lowered into the right NAcc (shell) (AP: +1.6 mm, ML: +2.2 mm from bregma, DV: 7.0–7.5 mm from the dural surface) and recording was started 90 min after implantation of the electrode. The optogenetic stimulation protocol was similar to the one used during fMRI and SPECT (10 trains, 10 pulses, 25 Hz, 10 ms, 10 mW, 532 nm in case of less-specific stimulation, 473 nm in case of specific stimulation).

Fast-scan cyclic voltammetry (FSCV) was performed with polymer-encased carbon fiber electrodes (7 µm diameter, ~100 µm length; Toray Carbon Fibers America, Inc., Santa Ana, CA, USA) as an acute procedure. The Ag/AgCl reference electrode was prepared from silver wires (0.5 mm diameter, Sigma-Aldrich, St Louis, MO, USA) chloridized in 0.1 M HCl. All cyclic voltammograms were obtained with a triangular waveform (scan rate: 10 Hz, resting potential: − 0.4 V, switching potential: 1.2 V, 400 V/s, 1000 samples per scan). Waveform generation and data collection were performed with the Invilog Voltammetric System and Software (Acquisition and Stimulation A&S, Invilog Research Ltd, Kuopio, Finland) and analyzed by a Fast Cyclic Voltammetry Analysis (FSV Analysis, Invilog Research Ltd, Kuopio, Finland) tool, which integrates FSCV and displays electrochemical measurements on a base station computer.

Because of the inherent differences in sensitivity between Polymer-coated electrodes, *in vivo* changes in oxidation current recorded with different electrodes (in different animals) cannot be assumed to be equivalent. Thus, valid comparisons are possible only if the sensitivity of each electrode is calibrated against a standard and the electrochemical data are expressed as standard equivalent values. In the present study, DA was used as the standard to calibrate the working electrode sensitivity. Accordingly, *in vivo* changes in oxidation current are expressed as µM values of dopamine concentration. Therefore, the peak oxidation currents for dopamine in each voltammogram (at approximately 0.6 V) were converted into concentration from a post-experiment calibration against fresh solutions of 0.1–2 µM dopamine.

Histology

Rats were perfused transcardially and the brain was sectioned on a vibratome or cryostat. Fiber placement and viral expression were confirmed under a confocal microscope. Primary antibody against tyrosine hydroxylase (1:1000 rabbit anti-TH, Milipore) and fluorescent (Alexa 546, Molecular Probes) secondary anti-rabbit antibody were used to stain for dopaminergic cells. The locations of fiber tips in individual animals are shown in Fig. S3. In three exemplary animals the fraction of dopaminergic (Th-expressing) and non-dopaminergic construct expressing cells were counted using the ImageJ cell-counting plugin (Fig. S4).

Results

Intracranial self-stimulation is acquired at comparable levels in groups receiving less-specific and dopamine specific optogenetic stimulation

In order to exclude strong differences in the behavioral impact of different optogenetic stimulation, we quantified the rewarding effects of stimulation using optogenetic intracranial self-stimulation (optoICSS). Two groups of animals were used: (A) a dopamine specific paradigm, in which channelrhodopsin is expressed exclusively in dopaminergic VTA neurons of Th-Cre rats and (B) a less-specific paradigm, in which channelrhodopsin is expressed under the CamKIIa-promoter and hence in a mixed population of the VTA neurons, comprising dopaminergic and glutamatergic cells, in wild-type littermates. Animals were placed in the self-stimulation chamber for 30 min once per day (Fig. 1 A), where they could evoke optical VTA stimulation by pressing a nose poke (25 Hz, 10 ms per pulse, 10 mW intensity at the tip of the fiber). ICSS mean press rates for the both groups of animals were not significantly different (Wilcoxon rank sum test on the means over consecutive days, $p = 0.375$) and also the time course of acquisition was remarkably similar between them (Fig. 1C). This finding confirms that the two optogenetic paradigms had a similar appetitive behavioral impact despite their differing specificities.

Only less-specific VTA activation causes widespread BOLD responses in the rat brain

Animals in all three groups, two optogenetic and one electrical group, were subjected to identical fMRI measurements. In electrically stimulated animals, BOLD signal intensity changes were present in multiple regions such as the ipsilateral VTA/substantia nigra, prefrontal cortex,

anterior cingulate cortex, inferior colliculus and thalamus (Fig. 2 A). The magnitude of BOLD changes in these areas was the highest among all groups. Of note, nucleus accumbens did not show a clear BOLD response to stimulation.

Less-specific optogenetic VTA stimulation also elicited detectable BOLD responses in the same structures which were activated by electrical stimulation (Fig. 2 A, B). However, the magnitude of BOLD responses was lower compared to electrical stimulation. Similar to our previously reported findings on electrical VTA stimulation (Helbing et al., 2016), the activity induced by less-specific stimulation was not attenuated in the presence of the dopamine $D_{1/5}$ receptor antagonist SCH23390 as confirmed by a second-level analysis (Fig. S1).

In stark contrast to electrical and less-specific stimulation, we found only weak BOLD responses in the group with specific stimulation. Significant responses were absent in the aforementioned reward-related areas and only some activity was present in the tectal region, an area not associated with reward processing (Fig. 2 A). This finding is in apparent contrast to results from other groups (Ferenczi et al., 2016; Lohani et al., 2016) but confirms our previously reported observations (Helbing et al., 2016). To resolve this discrepancy, we repeated our analysis with a reduced statistical threshold and without correction for multiple comparisons (Fig. 2 A, right panel). Under these circumstances we found significant activations in the ipsilateral nucleus accumbens, the dorsal striatum and the mentioned tectal activation.

In EYFP control animals (n = 2), almost no activity was present. A weak increase of BOLD signal was only evident in a small part of the thalamus. This region corresponds to an area which also became active in the specific stimulation paradigm, but the magnitude of the response was lower. It is likely, that the activation is due to visual stimulation from unavoidable stray light.

Strong dopamine release in NAcc evoked by optogenetic VTA stimulation

While the behavioral equivalence of both optogenetic stimulation groups indicates a similar level of appetitive dopamine release, the time course of the release remains unknown. We therefore performed fast-scan cyclic voltammetry (FSCV) in optogenetically stimulated animals. In both groups (less-specific and specific stimulation) we found significant dopamine release in NAcc (Fig. 3 D). The release faithfully followed stimulation and did not lead to depletion of release or sustained high

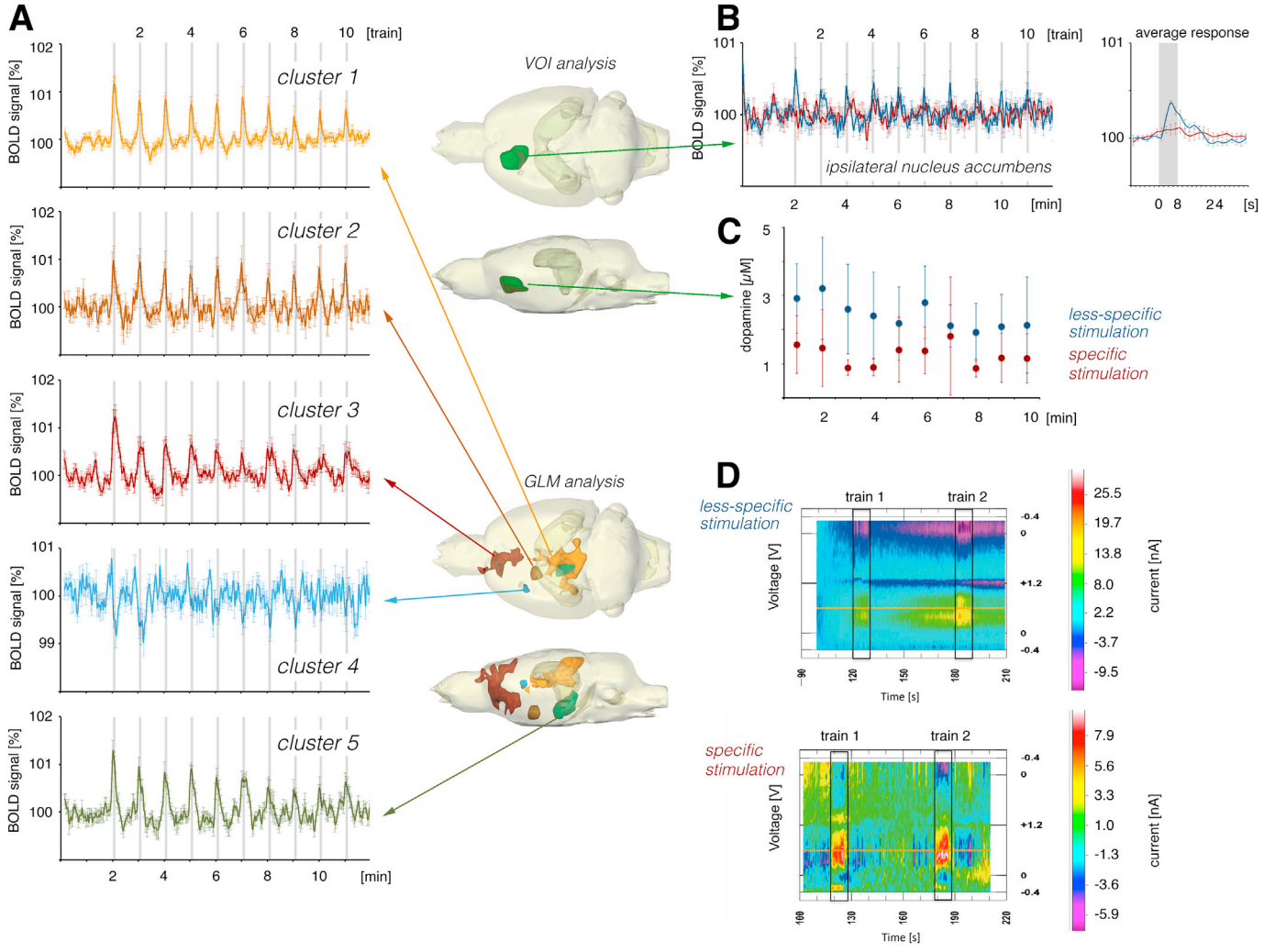

Fig. 3. Time course of BOLD responses and dopamine release. A: Temporal variation of stimulus-induced BOLD during ten consecutive stimulation trains in different activity clusters. Cluster 1: dorsal midbrain and tectum; cluster 2: ventromedial hypothalamic nucleus; cluster 3: prelimbic, infralimbic cingulate and dorsal peduncular cortex; cluster 4: part of dorsal striatum on ipsilateral side, cluster 5: ipsilateral VTA/substantia nigra. B: Temporal variations in BOLD signals in the ipsilateral nucleus accumbens (VOI analysis) during ten consecutive stimulation trains. C: FSCV of dopamine release into the contralateral nucleus accumbens during consecutive stimulation trains of the VTA in less-specific condition (n = 3, blue graph) and dopamine specific condition (n = 4, red graph). D: FSCV recordings in the contralateral nucleus accumbens during two consecutive stimulation periods. Please note the difference in scale bars, which is due to limitations in the used FSCV software.

levels of dopamine for at least ten consecutive stimulation trains, a prerequisite to detect associated BOLD signal changes (Fig. 3C).

Temporal dissociation between DA-release and BOLD signal

As described above, no canonical BOLD signal was elicited by specific stimulation but less-specific stimulation elicited a clear response throughout the brain. However, we found a strong decline in this response over consecutive stimulation trains (Fig. 3 A, Fig. S2). After approximately six repetitions, BOLD responses dropped below statistical threshold (Fig. S2). Responses around the stimulation site and in the tectal region were most stable, while responses in NAcc and mPFC declined first. This adaptation was not mirrored by the amount of dopamine releases in the NAcc over repeated stimulation trains as measured by FSCV (Fig. 3C). While the first two stimulation repetitions showed a small decline in release quantity, release was stable throughout remaining stimulation trains, both in the specific and less-specific paradigm. Thus, there exists a temporal dissociation between the strength of neurovascular responses and concurrently induced dopamine releases.

SPECT images of rCBF in awake animals mirror fMRI results

We used medetomidine for sedation during fMRI measurements. The neuronal activity patterns may thus differ from the awake state. To test the influence of our fMRI sedation protocol on stimulus-induced neurovascular responses to optogenetic stimulation, we employed ^{99m}Tc-HMPAO SPECT.

Using a protocol with continuous intravenous tracer-injection during ongoing behavior (Kolodziej et al., 2014) this approach allows obtaining images of spatial patterns of the regional cerebral blood flow in awake animals. ^{99m}Tc-HMPAO is a lipophilic compound that accumulates in the brain in a flow-dependent manner. After passing the blood-brain barrier, the compound is rapidly converted to a hydrophilic compound that remains trapped in the brain and shows no redistribution. Similar in rationale to ^{18}F-FDG-PET (Endepols et al., 2010) the distribution of the trapped tracer can be determined in anesthetized animals after stimulation. The images represent the spatial patterns of the average cerebral blood flow during the period of tracer-injection.

We performed the SPECT experiments on the same animals that were used during fMRI imaging to allow for a direct comparison. Similar to the results from fMRI, less-specific stimulation caused increased rCBF in the

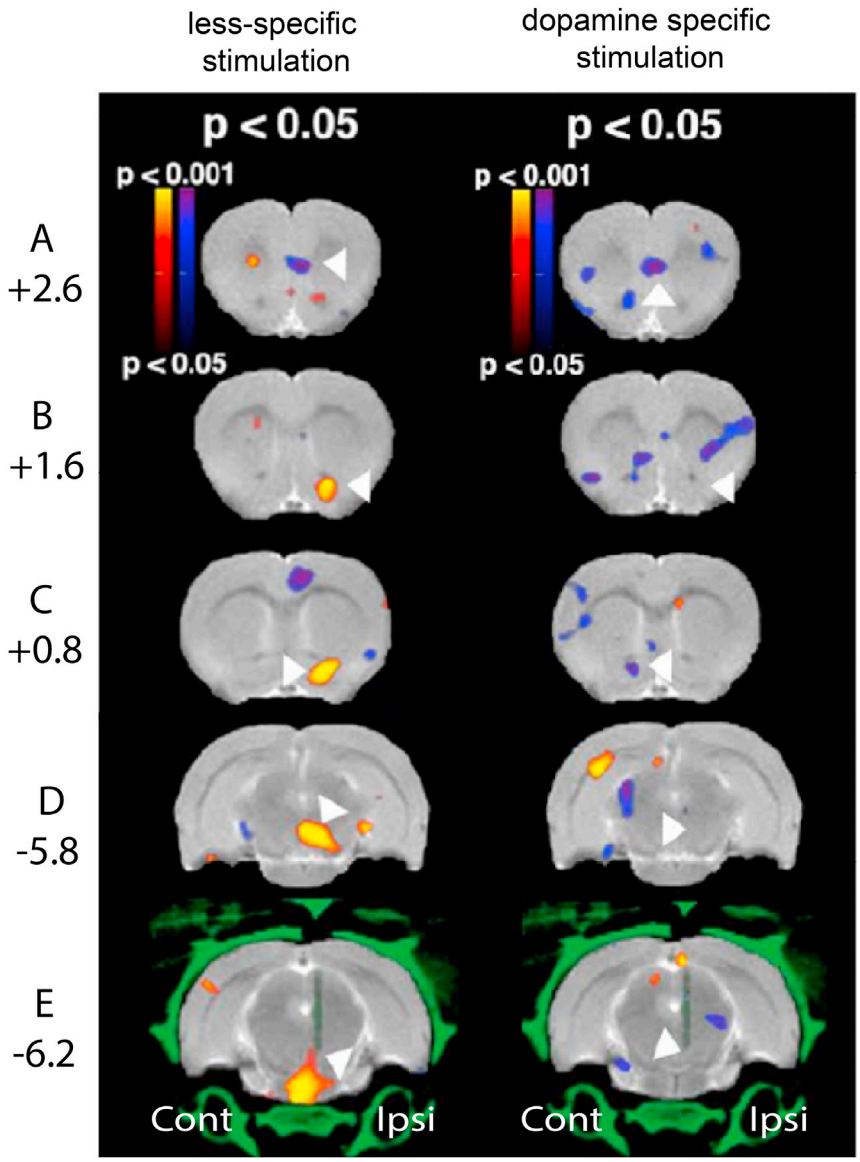

Fig. 4. rCBF SPECT imaging of optogenetic VTA stimulation in awake animals. Shown are maps of significant increases (red to yellow) and decreases (blue to violet) in uptake of the blood flow tracer 99mTcHMPAO under stimulus vs. baseline conditions, overlaid on a structural MR image and micro-CT (green). Tracer uptake increases significantly in the accumbens nucleus ipsilateral to the stimulation site during less-specific but not dopamine-specific stimulation (B,C). Furthermore, less-specific stimulation induces an increase in rCBF at the stimulation site (E). Marked with arrowheads: A: prelimbic/infralimbic cortex; B, C: ipsilateral NAcc; D: ipsilateral VTA; E: bilateral VTA/interpeduncular nucleus.

ipsilateral VTA and the neighboring interpeduncular nucleus. In addition, we found significantly increased rCBF in the ipsilateral nucleus accumbens and deactivation in frontal cortex (Fig. 4 A, B, C). In contrast to less-specific stimulation and in accordance to our fMRI results, specific stimulation did not induce detectable rCBF increases in these regions. Similar to less-specific stimulation, a reduction in frontal rCBF was present (Fig. 4 A).

Discussion

Here we investigate to what degree dopaminergic VTA neurons can drive neurovascular responses in reward related brain structures. We find that the contribution of dopamine neurons of the VTA to BOLD responses in the reward system is small. Therefore, canonical BOLD responses—as observed in human studies—are likely not primarily the result of dopaminergic activity but mediated through alternative routes, for example glutamatergic transmission. Understanding this type of neurovascular coupling on a mechanistic level is critical to meaningfully study the mesolimbic dopamine system in health and disease. Only thusly we can judge the usefulness of neurovascular responses in the reward system as markers for dopamine release, reward and value (D'Ardenne et al., 2007; da Silva Alves et al., 2011). In addition, deep-brain stimulation of dopaminergic tracts is an emerging treatment for several diseases, such as addiction (Müller et al., 2016), bipolar disorder (Gippert et al., 2017), obsessive-compulsive disorder (Coenen et al., 2017), and depression (Fenoy et al., 2016; Schulz and Arora, 2015). The link between neurovascular responses and dopamine release would therefore have great implications for the usefulness of functional imaging in measuring neural correlates of treatment response and our understanding of the causal mechanisms of such approaches.

A number of studies have previously investigated how dopaminergic neurons in the VTA affect neurovascular coupling mechanisms, for example using pharmacological approaches (Shih et al., 2009), drugs of addiction (Febo et al., 2004; Marota et al., 2000), fMRI combined with PET (Ghahremani et al., 2012; Schott et al., 2008; Urban et al., 2012), dopamine sensors (Lee et al., 2014) and electrical stimulation (Arsenault et al., 2014). More recent studies have also used optogenetic stimulation to more causally establish a link between dopamine release and BOLD (Ferenczi et al., 2016; Helbing et al., 2016; Lohani et al., 2016). In the majority of studies, a correlation between DA release and BOLD signal was reported but the magnitude of BOLD responses was surprisingly low (Ferenczi et al., 2016). However, dopamine neurons are not the only cells in the VTA (Fig. 5) and dopamine as a neuromodulator often lacks a clear driving influence on postsynaptic neurons. It is therefore possible that increased blood flow in NAcc and other VTA-linked structures is the result of a more complex process that rather depends on the release of different neurotransmitters from non-dopaminergic VTA cells or on direct influences of dopamine on the vasculature (Choi et al., 2006). For example, it has been suggested that the observed changes in BOLD signal intensities during stimulus-induced dopamine release may be rather driven by, for example, glutamatergic neurotransmission (Helbing et al., 2016; Ip et al., 2017; Urban et al., 2012). Glutamatergic transmission is responsible for a large part of the brains oxidative metabolism (Shen et al., 1999) and would be a natural candidate, particularly since glutamatergic cells are the major non-dopaminergic cell type targeted by our use of the CamKIIa-promoter in less-specific stimulation (Fig. S4). It is also possible that under specific circumstances dopamine receptors cause the shunting of excitatory postsynaptic currents, resulting in increased metabolic load and a BOLD response (Lippert et al., 2010). This response would depend, however, on the presence of a specific parallel activation instead of dopamine release itself.

According to the recent optogenetic studies (Decot et al., 2016; Ferenczi et al., 2016; Lohani et al., 2016), stimulation of dopaminergic VTA cells leads to an increase of BOLD signal intensities mostly in dorsal and ventral striatum (NAcc). Our recent results partially confirm these observations. We found that specific stimulation of dopaminergic VTA neurons results in minor increases of BOLD signal in dorsal striatum. This signal was not evenly distributed across the entire dorsal striatum, but rather scattered and therefore hardly detectable in a multi-subject GLM analysis. Using VOI analysis, i.e., considering all voxels in the left dorsal striatum we found BOLD signal increases in the range of 0.15%, which became only obvious by averaging the results of all trains in all animals. Considering the fact that for VOI analysis the resulting BOLD response is alleviated by non-responding voxels this result is comparable with previous reports (Ferenczi et al., 2016). Similarly, less-specific optical stimulation of VTA neurons resulted in an equally positive BOLD response but also in a subsequent negative BOLD response. This delayed negative response was the main response that was induced by electrical

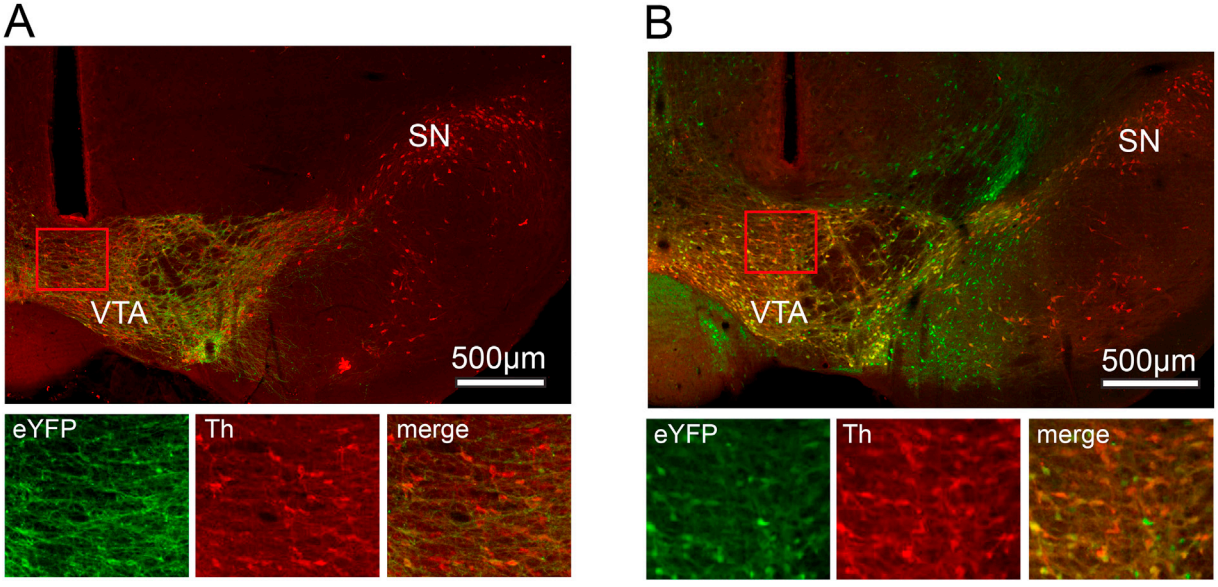

Fig. 5. Histological confirmation of fiber position and virus expression. A: Expression of the optogenetic construct (green) in Th-Cre animals (specific stimulation). Expression is confined to Th-positive, dopaminergic cells (red). B: Expression of the optogenetic construct (green) under CamKIIa-promoter in wild-type littermates (less-specific stimulation). In the stimulated region, expression is predominantly visible in Th-positive, dopaminergic cells (red), but also in a number of Th-negative, non-dopaminergic cells.

VTA stimulation; the initial positive response was missing. One explanation of this phenomenon might be that the negative response is a characteristic of non-dopaminergic processes, as it increases—and in the case of electrical stimulation potentially even masks the positive signal—with decreasing stimulation specificity. The small positive signal might therefore more reflect a dopamine-linked process in line with previous research (Decot et al., 2016; Ferenczi et al., 2016; Lohani et al., 2016). The positive component was observed in the ipsilateral and contralateral striatum, whereas a positive component was only observed in the ipsilateral but not in the contralateral NAcc. This agrees with recently described cross-hemispheric dopamine projections from the VTA to the dorsal and ventral striatum that were detected by in-vivo voltammetry in awake and anesthetized rats. In particular unilateral VTA stimulation triggered similar dopamine releases in the ipsi- and contralateral striatum whereas dopamine release in the contralateral NAcc was about 20 fold lower than in the ipsilateral Nacc (Fox et al., 2016). Nonetheless, although all three stimulation conditions resulted in clear activation of dopaminergic neurons in the VTA, as measured by *in vivo* fast scan cyclic-voltammetry (for voltammetry data from electrically stimulated animals see Helbing et al., 2016), each stimulation condition caused a different hemodynamic response in the dorsal striatum. Importantly, we found no strong BOLD responses in the direct projection targets of the VTA: ventral striatum (NAcc) and mPFC. In the mPFC, specific stimulation of dopaminergic neurons caused no significant variations in BOLD signals, whereas less-specific optical stimulation increased the BOLD signal by 0.5% and electrical stimulation by more than 1.0%, although it is difficult to compare activation strength across stimulation modality due to inherent differences in the underlying processes. This increase in BOLD signals was not affected by the dopamine $D_{1/5}$ receptor antagonist SCH23390 (Fig. S2, Helbing et al., 2016), indicating that dopaminergic transmission is not responsible for these BOLD signal changes. Even if the used field strength of 4.7T is insufficient to detect BOLD signal changes in the mPFC during specific stimulation, a clear qualitative difference in induced BOLD responses exists between specific and less-specific stimulation.

Therefore, we assume that the activity of non-dopaminergic cells is the main driver of the observed reward-related canonical BOLD response in, for example, human studies.

An interesting explanation for the weak, spatially restricted BOLD signal changes could be that the influence of dopamine on BOLD might even be mediated via non-neuronal processes. It has been demonstrated in that context that BOLD signal changes coupled with dopamine release are correlated with the expression of dopamine receptors on microvessels and astroglia rather than purely neuronal activity (Choi et al., 2006). In addition, co-release of glutamate from dopaminergic neurons could induce a small excitatory BOLD response (Stuber et al., 2010). It is therefore unclear whether the use of high field scanners or contrast agents brings to light a neuronal signal.

A critical factor in our experiments is the use of medetomidine to sedate the animals for fMRI measurements. BOLD responses might rely on the interaction of ongoing activity and dopamine release or other processes which are altered during sedation. We therefore conducted the rCBF SPECT experiments to address this concern. The results of these experiments suggest that in awake as well as in anesthetized animals the influence of dopaminergic neurons on dorsal and ventral striatal blood flow is weak. Again, only less-specific stimulation was able to induce detectable changes in blood flow. These results mirror our findings from fMRI and support the hypothesis that selective activation of dopaminergic VTA cells induces only weak neurovascular responses despite the strong behavioral response which is documented, for example, by the high rates of self-stimulation it induces. We attribute the deviations observed between fMRI and SPECT activation patterns to differences in the measured hemodynamic signal. SPECT measures rCBF and is sensitive to slow, long lasting shifts in blood flow, whereas fMRI BOLD measures blood oxygenation and is more sensitive towards tightly stimulus locked changes. The neurovascular signal in the ipsilateral NAcc—which was present in non-selectively stimulated animals in SPECT but not fMRI—for example, might be due to a slow continuous shift in neuronal activity or metabolism following repeated trains of VTA stimulation. Also, the small frontal deactivations found in the specific stimulation condition might be attributable to these causes. Functional SPECT imaging is therefore a valuable technique to image activities which are not easily detected by conventional fMRI BOLD.

In summary, our study shows that dopamine- and reward-related neuronal processes might not be unambiguously reflected by neurovascular signals measured during fMRI. In particular, mesolimbic dopamine release and concurrent changes of BOLD signals in structures of the reward network may not be causally related. While dopamine release can clearly drive behavior, its ability to drive BOLD responses might be significantly weaker than assumed. To monitor dopaminergic activity, either dopamine-sensitive MR contrast agents, such as BM3H (Lee et al., 2014; Shapiro et al., 2010) or a combination with PET should be considered.

Funding statement

This work was funded by the Leibniz-Society (LIN Special Project SAW-2015-LIN-3).

Acknowledgements

We thank Karla Krautwald, Ines Heinemann and Silvia Vieweg for their excellent technical assistance.

Appendix A. Supplementary data

Supplementary data related to this article can be found at https://doi.org/10.1016/j.neuroimage.2018.04.059.

References

Arsenault, J.T., Rima, S., Stemmann, H., Vanduffel, W., 2014. Role of the primate ventral tegmental area in reinforcement and motivation. Curr. Biol. 24, 1347–1353. https://doi.org/10.1016/j.cub.2014.04.044.

Beier, K.T., Steinberg, E.E., Deloach, K.E., Xie, S., Miyamichi, K., Schwarz, L., Gao, X.J., Kremer, E.J., Malenka, R.C., Luo, L., 2015. Circuit architecture of VTA dopamine neurons revealed by systematic input-output mapping. Cell 162, 622–634. https://doi.org/10.1016/j.cell.2015.07.015.

Choi, J.K., Chen, Y.I., Hamel, E., Jenkins, B.G., 2006. Brain hemodynamic changes mediated by dopamine receptors: role of the cerebral microvasculature in dopamine-mediated neurovascular coupling. Neuroimage 30, 700–712. https://doi.org/10.1016/j.neuroimage.2005.10.029.

Coenen, V.A., Schlaepfer, T.E., Goll, P., Reinacher, P.C., Voderholzer, U., Tebartz Van Elst, L., Urbach, H., Freyer, T., 2017. The medial forebrain bundle as a target for deep brain stimulation for obsessive-compulsive disorder. CNS Spectr. 22, 282–289. https://doi.org/10.1017/S1092852916000286.

D'Ardenne, K., McClure, S.M., Nystrom, L.E., Cohen, J.D., 2007. BOLD responses reflecting dopaminergic signals in the human ventral tegmental area. Science 342, 233–238.

da Silva Alves, F., Schmitz, N., Figee, M., Abeling, N., Hasler, G., van der Meer, J., Nederveen, A., de Haan, L., Linszen, D., van Amelsvoort, T., 2011. Dopaminergic modulation of the human reward system: a placebo-controlled dopamine depletion fMRI study. J. Psychopharmacol. 25, 538–549. https://doi.org/10.1177/0269881110367731.

Decot, H.K., Namboodiri, V.M.K., Gao, W., McHenry, J.A., Jennings, J.H., Lee, S.-H., Kantak, P.A., Jill Kao, Y.-C., Das, M., Witten, I.B., Deisseroth, K., Shih, Y.-Y.I., Stuber, G.D., 2016. Coordination of brain-wide activity dynamics by dopaminergic neurons. Neuropsychopharmacology 42, 615.

Endepols, H., Sommer, S., Backes, H., Wiedermann, D., Graf, R., Hauber, W., 2010. Effort-based decision making in the rat: an [18F]Fluorodeoxyglucose micro positron emission tomography study. J. Neurosci. 30, 9708–9714. https://doi.org/10.1523/JNEUROSCI.1202-10.2010.

Febo, M., Segarra, A.C., Tenney, J.R., Brevard, M.E., Duong, T.Q., Ferris, C.F., 2004. Imaging cocaine-induced changes in the mesocorticolimbic dopaminergic system of conscious rats. J. Neurosci. Methods 139, 167–176. https://doi.org/10.1016/j.jneumeth.2004.04.028.

Fenoy, A.J., Schulz, P., Selvaraj, S., Burrows, C., Spiker, D., Cao, B., Zunta-Soares, G., Gajwani, P., Quevedo, J., Soares, J., 2016. Deep brain stimulation of the medial forebrain bundle: distinctive responses in resistant depression. J. Affect. Disord. 203, 143–151. https://doi.org/10.1016/j.jad.2016.05.064.

Ferenczi, E.A., Zalocusky, K.A., Liston, C., Grosenick, L., Warden, M.R., Amatya, D., Katovich, K., Mehta, H., Patenaude, B., Ramakrishnan, C., Kalanithi, P., Etkin, A., Knutson, B., Glover, G.H., Deisseroth, K., 2016. Prefrontal cortical regulation of brainwide circuit dynamics and reward-related behavior. Science (80-.) 351 aac9698-aac9698. https://doi.org/10.1126/science.aac9698.

Fitch, T.E., Sahr, R.N., Eastwood, B.J., Zhou, F.C., Yang, C.R., Thomas, E., Feng, C., Dopamine, D., 2006. Dopamine D1/5 receptor modulation of firing rate and bidirectional theta burst firing in medial septal/vertical limb of diagonal band neurons in vivo. J. Neurophysiol. 2808–2820. https://doi.org/10.1152/jn.01210.2005.

Fox, M.E., Mikhailova, M.A., Bass, C.E., Takmakov, P., Gainetdinov, R.R., Budygin, E.A., Wightman, R.M., 2016. Cross-hemispheric dopamine projections have functional significance. Proc. Natl. Acad. Sci. 113, 6985–6990. https://doi.org/10.1073/pnas.1603629113.

Ghahremani, D.G., Lee, B., Robertson, C.L., Tabibnia, G., Morgan, A.T., De Shetler, N., Brown, A.K., Monterosso, J.R., Aron, A.R., Mandelkern, M.A., Poldrack, R.A., London, E.D., 2012. Striatal dopamine d2/d3 receptors mediate response inhibition and related activity in frontostriatal neural circuitry in humans. J. Neurosci. 32, 7316–7324. https://doi.org/10.1523/JNEUROSCI.4284-11.2012.

Gippert, S.M., Switala, C., Bewernick, B.H., Kayser, S., Bräuer, A., Coenen, V.A., Schlaepfer, T.E., 2017. Deep brain stimulation for bipolar disorder—review and outlook. CNS Spectr. 22, 254–257. https://doi.org/10.1017/S1092852915000577.

Goebel, R., 2012. BrainVoyager - past, present, future. Neuroimage 62, 748–756. https://doi.org/10.1016/j.neuroimage.2012.01.083.

Guo, S., Chen, S., Zhang, Q., Wang, Y., Xu, K., Zheng, X., 2014. Optogenetic activation of the excitatory neurons expressing CaMKIIa in the ventral tegmental area upregulates the locomotor activity of free behaving rats. Biomed. Res. Int. 2014 https://doi.org/10.1155/2014/687469.

Helbing, C., Brocka, M., Scherf, T., Lippert, M.T., Angenstein, F., 2016. The role of the mesolimbic dopamine system in the formation of blood-oxygen-level dependent responses in the medial prefrontal/anterior cingulate cortex during high-frequency stimulation of the rat perforant pathway. J. Cereb. Blood Flow. Metab. 36, 2177–2193. https://doi.org/10.1177/0271678X15615535.

Hnasko, T.S., Hjelmstad, G.O., Fields, H.L., Edwards, R.H., 2012. Ventral tegmental area glutamate neurons: electrophysiological properties and projections. J. Neurosci. 32, 15076–15085. https://doi.org/10.1523/JNEUROSCI.3128-12.2012.

Honey, G.D., Suckling, J., Zelaya, F., Long, C., Routledge, C., Jackson, S., Ng, V., Fletcher, P.C., Williams, S.C.R., Brown, J., Bullmore, E.T., 2003. Dopaminergic drug effects on physiological connectivity in a human cortico-striato-thalamic system. Brain 126, 1767–1781. https://doi.org/10.1093/brain/awg184.

Ip, B., Berrington, A., Hess, A.T., Parker, A.J., Emir, U.E., Bridge, H., 2017. Combined fMRI-MRS acquires simultaneous glutamate and BOLD-fMRI signals in the human brain. Neuroimage 155, 113–119. https://doi.org/10.1016/j.neuroimage.2017.04.030.

Knutson, B., Gibbs, S.E.B., 2007. Linking nucleus accumbens dopamine and blood oxygenation. Psychopharmacol. Berl. 191, 813–822. https://doi.org/10.1007/s00213-006-0686-7.

Kolodziej, A., Lippert, M., Angenstein, F., Neubert, J., Pethe, A., Grosser, O.S., Amthauer, H., Schroeder, U.H., Reymann, K.G., Scheich, H., Ohl, F.W., Goldschmidt, J., 2014. SPECT-imaging of activity-dependent changes in regional cerebral blood flow induced by electrical and optogenetic self-stimulation in mice. Neuroimage 103, 171–180. https://doi.org/10.1016/j.neuroimage.2014.09.023.

Kufahl, P.R., Li, Z., Risinger, R.C., Rainey, C.J., Wu, G., Bloom, A.S., Li, S.J., 2005. Neural responses to acute cocaine administration in the human brain detected by fMRI. Neuroimage 28, 904–914. https://doi.org/10.1016/j.neuroimage.2005.06.039.

Kunori, N., Kajiwara, R., Takashima, I., 2014. Voltage-sensitive dye imaging of primary motor cortex activity produced by ventral tegmental area stimulation. J. Neurosci. 34, 8894–8903. https://doi.org/10.1523/JNEUROSCI.5286-13.2014.

Lee, T., Cal, L.X., Lelyveld, V.S., Hai, A., Jasanoff, A., 2014. Molecular-level functional magnetic resonance imaging of dopaminergic signaling. Science 344, 533–536. https://doi.org/10.1126/science.1249380.

Li, Y., Fang, F., Wang, X., Lei, H., 2009. Neuronal projections from ventral tegmental area to forebrain structures in rat studied by manganese-enhanced magnetic resonance imaging. Magn. Reson. Imaging 27, 293–299. https://doi.org/10.1016/j.mri.2008.07.011.

Lippert, M.T., Steudel, T., Ohl, F., Logothetis, N.K., Kayser, C., 2010. Coupling of neural activity and fMRI-BOLD in the motion area MT. Magn. Reson. Imaging 28, 1087–1094. https://doi.org/10.1016/j.mri.2009.12.028.

Lohani, S., Poplawsky, A.J., Seong-Gi, K., Mohhhaddam, B., Group, L.I., Diego, S., 2016. Unexpected global impact of VTA dopamine neuron activation as measured by opto-fMRI. Mol. Psychiatry 36, 1011–1014 . https://doi.org/10.1002/jmri.23741.Proton.

Marota, J.J., Mandeville, J.B., Weisskoff, R.M., Moskowitz, M.a, Rosen, B.R., Kosofsky, B.E., 2000. Cocaine activation discriminates dopaminergic projections by temporal response: an fMRI study in Rat. Neuroimage 11, 13–23. https://doi.org/10.1006/nimg.1999.0520.

Michaelides, M., Anderson, S.A.R., Ananth, M., Smirnov, D., Thanos, P.K., Neumaier, J.F., Wang, G.J., Volkow, N.D., Hurd, Y.L., 2013. Whole-brain circuit dissection in free-moving animals reveals cell-specific mesocorticolimbic networks. J. Clin. Invest. 123, 5342–5350. https://doi.org/10.1172/JCI72117.

Müller, U.J., Sturm, V., Voges, J., Heinze, H.-J., Galazky, I., Büntjen, L., Heldmann, M., Frodl, T., Steiner, J., Bogerts, B., 2016. Nucleus accumbens deep brain stimulation for alcohol addiction – safety and clinical long-term results of a pilot trial. Pharmacopsychiatry 49, 170–173. https://doi.org/10.1055/s-0042-104507.

Ohlstein, E.H., Berkowitz, B.A., 1985. SCH 23390 and SK&F 83566 are antagonists at vascular dopamine and serotonin receptors. Eur. J. Pharmacol. 108, 205–208. https://doi.org/https://doi.org/10.1016/0014-2999(85)90728-9.

Prakash, R., Yizhar, O., Grewe, B., Ramakrishnan, C., Wang, N., Goshen, I., Packer, A.M., Peterka, D.S., Yuste, R., Schnitzer, M.J., Deisseroth, K., 2012. Two-photon optogenetic toolbox for fast inhibition, excitation and bistable modulation. Nat. Methods 9, 1171–1179. https://doi.org/10.1038/nmeth.2215.

Sanchez-Catalan, M.J., Kaufling, J., Georges, F., Veinante, P., Barrot, M., 2014. The antero-posterior heterogeneity of the ventral tegmental area. Neuroscience 282, 198–216. https://doi.org/10.1016/j.neuroscience.2014.09.025.

Schott, B.H., Minuzzi, L., Krebs, R.M., Elmenhorst, D., Lang, M., Winz, O.H., Seidenbecher, C.I., Coenen, H.H., Heinze, H.-J., Zilles, K., Duzel, E., Bauer, A., 2008. Mesolimbic functional magnetic resonance imaging activations during reward anticipation correlate with reward-related ventral striatal dopamine release. J. Neurosci. 28, 14311–14319. https://doi.org/10.1523/JNEUROSCI.2058-08.2008.

Schultz, W., Dayan, P., Montague, P.R., 1997. A neural substrate of prediction and reward. Science 275 (80), 1593–1599. https://doi.org/10.1126/science.275.5306.1593.

Schulz, P.E., Arora, G., 2015. Depression. Contin. Lifelong learn. Neurol. 21.

Shapiro, M.G., Westmeyer, G.G., Romero, P.A., Szablowski, J.O., Küster, B., Shah, A., Otey, C.R., Langer, R., Arnold, F.H., Jasanoff, A., 2010. Directed evolution of a magnetic resonance imaging contrast agent for noninvasive imaging of dopamine. Nat. Biotechnol. 28, 264.

Shen, J., Petersen, K.F., Behar, K.L., Brown, P., Nixon, T.W., Mason, G.F., Petroff, O. a, Shulman, G.I., Shulman, R.G., Rothman, D.L., 1999. Determination of the rate of the glutamate/glutamine cycle in the human brain by in vivo 13C NMR. Proc. Natl. Acad. Sci. U. S. A. 96, 8235–8240. https://doi.org/10.1073/pnas.96.14.8235.

Shih, Y.-Y.I., Chen, C.-C.V., Shyu, B.-C., Lin, Z.-J., Chiang, Y.-C., Jaw, F.-S., Chen, Y.-Y., Chang, C., 2009. A new scenario for negative functional magnetic resonance imaging signals: endogenous neurotransmission. J. Neurosci. 29, 3036–3044. https://doi.org/10.1523/JNEUROSCI.3447-08.2009.

Sokoloff, P., Leriche, L., Le Foll, B., 1988. Dopamine receptors: structure, function and implication in psychiatric disorders. Gene 357–419.

Solt, K., Van Dort, C., Chemali, J., Taylor, N.E., 2014. Electrical stimulation of the ventral tegmental area induces reanimation from general anesthesia. Anesthesiology 121, 311–319. https://doi.org/10.1097/ALN.0000000000000117.Electrical.

Steinberg, E.E., Keiflin, R., Boivin, J.R., Witten, I.B., Deisseroth, K., Janak, P.H., 2013. A causal link between prediction errors, dopamine neurons and learning. Nat. Neurosci. 16, 966–973. https://doi.org/10.1038/nn.3413.

Stuber, G.D., Hnasko, T.S., Britt, J.P., Edwards, R.H., Bonci, A., 2010. Dopaminergic terminals in the nucleus accumbens but not the dorsal striatum corelease glutamate. J. Neurosci. 30, 8229–8233. https://doi.org/10.1523/JNEUROSCI.1754-10.2010.

Taylor, N.E., Van Dort, C.J., Kenny, J.D., Pei, J., Guidera, J.A., Vlasov, K.Y., Lee, J.T., Boyden, E.S., Brown, E.N., Solt, K., 2016. Optogenetic activation of dopamine neurons in the ventral tegmental area induces reanimation from general anesthesia. Proc. Natl. Acad. Sci. 113, 12826–12831. https://doi.org/10.1073/pnas.1614340113.

Taylor, S.R., Badurek, S., Dileone, R.J., Nashmi, R., Minichiello, L., Picciotto, M.R., 2014. GABAergic and glutamatergic efferents of the mouse ventral tegmental area. J. Comp. Neurol. 522, 3308–3334. https://doi.org/10.1002/cne.23603.

Thanos, P.K., Robison, L., Nestler, E.J., Kim, R., Michaelides, M., Lobo, M.-K., Volkow, N.D., 2013. Mapping brain metabolic connectivity in awake rats with PET and optogenetic stimulation. J. Neurosci. 33, 6343–6349. https://doi.org/10.1523/JNEUROSCI.4997-12.2013.

Ungless, M.A., Argilli, E., Bonci, A., 2010. Effects of stress and aversion on dopamine neurons: implications for addiction. Neurosci. Biobehav. Rev. 35, 151–156. https://doi.org/10.1016/j.neubiorev.2010.04.006.

Urban, N.B.L., Slifstein, M., Meda, S., Xu, X., Ayoub, R., Medina, O., Pearlson, G.D., Krystal, J.H., Abi-Dargham, A., 2012. Imaging human reward processing with positron emission tomography and functional magnetic resonance imaging. Psychopharmacol. Berl. 221, 67–77. https://doi.org/10.1007/s00213-011-2543-6.

Vincenz, D., Wernecke, K.E.A., Fendt, M., Goldschmidt, J., 2017. Habenula and interpeduncular nucleus differentially modulate predator odor-induced innate fear behavior in rats. Behav. Brain Res. 332, 164–171. https://doi.org/10.1016/j.bbr.2017.05.053.

Volman, S.F., Lammel, S., Margolis, E.B., Kim, Y., Richard, J.M., Roitman, M.F., Lobo, M.K., 2013. New insights into the specificity and plasticity of reward and aversion encoding in the mesolimbic system. J. Neurosci. 33, 17569–17576. https://doi.org/10.1523/JNEUROSCI.3250-13.2013.

Vytlacil, J., Kayser, A., Miyakawa, A., D'Esposito, M., 2014. An approach for identifying brainstem dopaminergic pathways using resting state functional MRI. PLoS One 9, 1–7. https://doi.org/10.1371/journal.pone.0087109.

Walsh, J.J., Han, M.H., 2014. The heterogeneity of ventral tegmental area neurons: projection functions in a mood-related context. Neuroscience 282, 101–108. https://doi.org/10.1016/j.neuroscience.2014.06.006.

Weber, R., Ramos-Cabrer, P., Wiedermann, D., Van Camp, N., Hoehn, M., 2006. A fully noninvasive and robust experimental protocol for longitudinal fMRI studies in the rat. Neuroimage 29, 1303–1310. https://doi.org/10.1016/j.neuroimage.2005.08.028.

Wise, R.A., Koob, G.F., 2014. The development and maintenance of drug addiction. Neuropsychopharmacology 39, 254–262. https://doi.org/10.1038/npp.2013.261.

Witten, I.B., Steinberg, E.E., Lee, S.Y., Davidson, T.J., Zalocusky, K.A., Brodsky, M., Yizhar, O., Cho, S.L., Gong, S., Ramakrishnan, C., Stuber, G.D., Tye, K.M., Janak, P.H., Deisseroth, K., 2011. Recombinase-driver rat lines: tools, techniques, and optogenetic application to dopamine-mediated reinforcement. Neuron 72, 721–733. https://doi.org/10.1016/j.neuron.2011.10.028.

Yetnikoff, L., Lavezzi, H.N., Reichard, R.A., Zahm, D.S., 2014. An update on the connections of the ventral mesencephalic dopaminergic complex. Neuroscience 282, 23–48. https://doi.org/10.1016/j.neuroscience.2014.04.010.